Engineering Structures 172 (2018) 239–252

Contents lists available at ScienceDirect

Engineering Structures

journal homepage: www.elsevier.com/locate/engstruct

General solution for shear strength estimate of RC elements based on panel response

Leonardo M. Massone[a,*], Francisco Melo[b]

[a] Department of Civil Engineering, University of Chile, Blanco Encalada 2002, Santiago, Chile
[b] University of Chile, Chile

ARTICLE INFO

Keywords:
Shear strength
Panel response
Wall
Beam
Corbel
Beam-column joint

ABSTRACT

The capacity of structural systems subjected to shear loads commonly distinguished by discontinuities such as point loads or supports, or abrupt changes of cross section, where complex fields of stresses and strains are generated, is vital information for design. Four structural systems that present stress concentration due to applied shear loads are commonly short walls, deep beams, corbels and beam-column joints. In the present work a model is developed to predict the shear capacity of these elements based on a panel model that considers average strain and stresses in a reinforced concrete orthotropic material, which covers the section of the structural element subjected to stress concentration. In addition, the panel element complies with the longitudinal equilibrium, by equalizing the applied axial load with the internal stresses of the structural element, requiring constitutive material laws for both concrete and steel reinforcement. The original model that has shown good shear strength prediction requires solving the non-linear equation of vertical equilibrium. Thus, this work eliminates the need to solve the iterative problem for the capacity estimation of four possible limit states (failure of concrete in tension and compression, and yielding of longitudinal web and boundary reinforcement). For that, an expression is calibrated for the strain of the model with respect to relevant parameters, for each limit state, that allow the generation of a non-iterative model. The model results in an average predicted capacity over experimental capacity ratio, V_{model}/V_{test}, of 1.0 and a COV of 0.25, with similar performance for all four structural systems. When comparing these results with the general model that requires an iterative method, a similar performance is observed, with an average strength ratio and COV of 0.98 and 0.23, respectively. Likewise, in comparison with the ACI 318, the latter shows worse predictions (on average 24% lower) and with greater scatter (on average 28% higher). The expression in AASHTO code presents better correlation than ACI with predictions closer the proposed model.

1. Introduction

The capacity of structural systems subjected to shear loads is hindered by discontinuities such as point loads or supports, or abrupt changes of cross section, where complex fields of stresses and strains are developed. The shear loads, for these cases, generate a diagonal compression stress field in the concrete from the point of application of the load to the support, which is balanced by the tensile forces generated in the reinforcement and, to a lesser extent, in the concrete. Four structural systems that commonly present stress concentration due to applied shear loads are short walls (common in nuclear plants, facades and at the parking level in buildings), deep beams (coupling beams), corbels (elements that support beams, transferring loads to columns in precast systems) and beam-column joints (continuity element in frame structures).

Several models have been developed to calculate the shear capacity of structural systems, which are separated into two groups: theoretical and empirical (or semi-empirical). The empirical models are based purely on the correlation of experimentally determine capacities with respect to an expression with relevant parameters of the phenomenon (e.g., concrete compression strength, reinforcement yielding, aspect ratio). Expressions of this type were incorporated in the 60s on the ACI 318 standard [1] to estimate shear capacity, which were developed after the 1955 air-force warehouse shear failure [2]. However, these types of expressions are limited based on the experimental data used for the calibration. Due to this limitation, in ACI 318 of 1995 [3] a large number of over 40 expressions for shear strength estimation for different elements and load types have been included, which makes imperative to develop models with a theoretical basis that allow covering a broad spectrum of structural elements and parameter ranges [4]. The

* Corresponding author.
E-mail address: lmassone@ing.uchile.cl (L.M. Massone).

https://doi.org/10.1016/j.engstruct.2018.06.038
Received 22 December 2017; Received in revised form 1 May 2018; Accepted 10 June 2018
Available online 15 June 2018

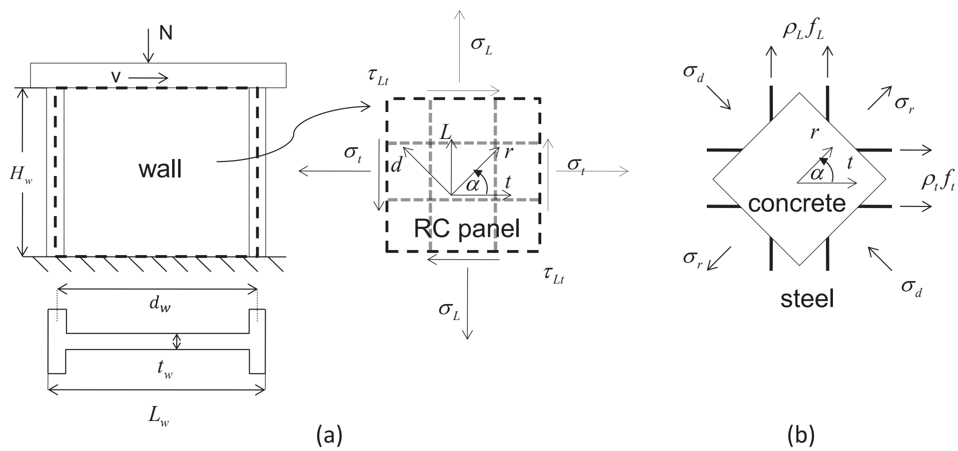

Fig. 1. Short wall – (a) Stress resultants in L–t coordinates, and (b) Stress resultants in principal direction d–r coordinates, including distributed reinforcement (after [9,10]).

understanding of shear response improved considerable with the development of panel constitutive law for cracked reinforced concrete. One of the first complete approaches was the Modified Compression Field Theory [5]. This model uses a rotating-angle modeling approach to describe the evolution of concrete average stress field that rotates as the external actions change, provided that the principal concrete stress direction coincide with the principal strain direction. Constitutive stress-strain models for materials are applied along the principal directions of the strain field in order to obtain the stress field associated with the principal directions. One of the relevant considerations of the panel or membrane model is the incorporation of the compression softening effect. The softening effect is mainly a reduction in the compressive stress of concrete along the principal compressive direction undergoing tensile strains in the other principal direction. The application of this and other membrane models has led to development of finite element formulation for detail reinforced concrete elements or structural analysis (e.g., Vecchio [6]), but also to simplified approaches for shear strength estimation (e.g., Collins et al. [4]).

Regarding theoretical models or based on the physics of the problem, there are two of the most accepted models to predict the shear capacity of structural elements: (i) softened truss or panel model (e.g., Hsu and Mo [7], Collins et al. [4]), and the softened strut-and-tie model (e.g., Hwang et al. [8]), some of them originally applied for walls. The softened truss model differs from the strut-and-tie model by the way the reinforcement and concrete stresses are incorporated in its formulation. The softened truss model assumes that each point of the structural element meets the stress equilibrium with a uniform distribution of stresses and strains. In contrast, softened strut-and-tie model simulates the force distribution in the structural element, with diagonal compression struts that represent the compressive stresses generated in concrete and tensile tensors that represent the stresses induced in the reinforcement. Thus, the model equilibrium is satisfied by the joint action of the strut-and-tie (lattice) system. The softened truss model presents a relatively simple formulation, where the hypothesis of uniform stresses simplifies the analysis. On the other hand, although the strut-and-tie model analyzes the phenomenon with a more convincing concept of stress flow, its formulation is more complex and highly dependent on the expression used to define the cross-sectional area of the compression strut.

In the present work, a closed-form solution (series of expressions that require no iterative numerical procedure for the strength estimate) for a softened truss model applicable to short walls, deep beams, corbels and beam-column joints is developed, based on the formulation proposed by Kassem and Elsheikh [9], originally for short walls, and which has been modified to generalize it and make it applicable to more structural systems [10–12]. Finally, the results of the modified model are compared with experimental results of the literature and with the code expressions of the ACI 318. The relevance of the article is not only showing that a simple material formulation based on general principles can correctly predict the shear strength of reinforced concrete elements for a large database (635 tests), but also that the iterative procedure (nonlinear equilibrium equation) can be avoided after a fitting analysis that keeps three main parameters such as axial load, material strength and principal concrete stress/strain direction, maintaining the main physics of the problem, such as the shear equilibrium equations, compatibility and material constitutive laws.

2. Base model and previous modifications

The base model developed by Kassem and Elsheikh [9], called the fixed-angle panel model, considers a softened truss model to estimate shear capacity for short walls. Geometrically, the model is detailed as shown in Fig. 1, where a short wall of height H_w, length L_w, effective length d_w (horizontal length of the short wall between the centroids of the boundary elements or calculated as $0.8L_w$ for non-barbell walls) and thickness t_w is subjected to an axial load N and another shear V. The short wall is analyzed as a panel element, in which the forces are uniform with respect to its axes. Two coordinate systems are considered, the "L–t" axes that follow the orientation of the longitudinal and transverse reinforcement of the structural element (Fig. 1a), and the "d–r" axes inclined at an angle α representing the slope of the compression diagonal strut developed in concrete (the angle represents the concrete stress principal direction) or principal strain direction angle (Fig. 1b), which is named in this article as principal direction angle. Thus, the normal stresses (σ_L, σ_t) and shear stress (τ_{Lt}) of the structural element are defined by the stresses of the coordinate system "L–t", calculated according to the responses of the distributed longitudinal reinforcement ($\rho_L f_L$) and distributed transverse reinforcement ($\rho_t f_t$), defined by their steel ratio (ρ_L, ρ_t) and average steel reinforcement stress (f_L, f_t) in the L or t direction, and the principal concrete stresses of the compression (σ_d) and tension (σ_r) directions that are in the coordinate system "d–r". All stresses are considered as average values within the panel.

For its formulation, the work by Kassem and Elsheikh [9] applies the equations of equilibrium of the system, strain compatibility and constitutive laws of both concrete and reinforcing steel. For this, it imposes a fixed angle for the principal strain direction that coincides with the principal concrete stress direction. This angle is determined as the one that better predicts the shear capacity of short walls for a database of 100 tests.

2.1. Stress transformation and strain compatibility

The equilibrium equations along the coordinate axis Lt are based on the principal direction concrete stresses. Since average stress fields are considered and the model formulation is described in the principal concrete stress direction, no stress check is imposed at the crack direction for local stresses, simplifying the approach. Thus, the equilibrium equations are defined as (Fig. 1):

$$\sigma_L = \sigma_d \cos^2\alpha + \sigma_r \sin^2\alpha + \rho_L f_L \tag{1}$$

$$\sigma_t = \sigma_d \sin^2\alpha + \sigma_r \cos^2\alpha + \rho_t f_t \tag{2}$$

$$\tau_{Lt} = (-\sigma_d + \sigma_r)\cos\alpha\sin\alpha \tag{3}$$

For uniform stress distribution within the panel, the shear force (V) is defined as,

$$V = \tau_{Lt} t_w d_w \tag{4}$$

Under the perfect adherence assumption between concrete and steel, the compatibility equations between L-t and d–r system become,

$$\varepsilon_L = \varepsilon_d \cos^2\alpha + \varepsilon_r \sin^2\alpha \tag{5}$$

$$\varepsilon_t = \varepsilon_d \sin^2\alpha + \varepsilon_r \cos^2\alpha \tag{6}$$

$$\gamma_{Lt} = 2(-\varepsilon_d + \varepsilon_r)\cos\alpha\sin\alpha \tag{7}$$

where ε_L, ε_t are the strain values in directions L and t, respectively; γ_{Lt} is the shear strain in the plane L–t; ε_d, ε_r are the principal strain values (positive for tensile). Finally, the top lateral shear displacement is determined as,

$$\Delta = \gamma_{Lt} H_w \tag{8}$$

2.2. Constitutive material laws

In order to determine the compressive stress in concrete (Fig. 2a, Eqs. (9)–(11)), the constitutive law proposed by Zhang and Hsu [13] is used, which considers softening of strength due to tensile strains in the perpendicular direction (ε_r) as (solid line–dashed line does not include the softening effect),

$$\sigma_d = -\xi f'_c\left[2\left(\frac{-\varepsilon_d}{\xi\varepsilon_o}\right) - \left(\frac{-\varepsilon_d}{\xi\varepsilon_o}\right)^2\right] \quad \text{if} \quad \varepsilon_d \leqslant \xi\varepsilon_o \tag{9}$$

$$\sigma_d = -\xi f'_c\left[1 - \left(\frac{\frac{-\varepsilon_d}{\xi\varepsilon_o} - 1}{\frac{2}{\xi} - 1}\right)^2\right] \text{ if } \xi\varepsilon_o < \varepsilon_d \leqslant 2\varepsilon_o \tag{10}$$

$$\xi = \frac{5.8}{\sqrt{f'c}}\frac{1}{\sqrt{1 + 400\varepsilon_r}} \leqslant \frac{0.9}{\sqrt{1 + 400\varepsilon_r}} \tag{11}$$

where ξ is the reduction coefficient; f'_c is the concrete compressive strength [MPa] for a consistent strain of $\varepsilon_o = 0.002$.

The tension behavior of concrete (Fig. 2b) is defined by the material law proposed by Gupta and Rangan [14] as,

$$\sigma_r = E_c \varepsilon_r \text{ if } 0 \leqslant \varepsilon_r \leqslant \varepsilon_{ct} \tag{12}$$

$$\sigma_r = f'_{ct}\left(\frac{\varepsilon_{ut} - \varepsilon_r}{\varepsilon_{ut} - \varepsilon_{ct}}\right) \text{ if } \varepsilon_{ct} < \varepsilon_r \leqslant \varepsilon_{ut} \tag{13}$$

where $f'_{ct} = 0.4\sqrt{f'_c[MPa]}$ is the tensile strength; $E_c = 4700\sqrt{f'_c[MPa]}$ is the concrete elastic modulus; $\varepsilon_{ct} = f'_{ct}/E_c$ is the cracking strain and $\varepsilon_{ut} = 0.002$ is the ultimate tensile strain.

The reinforcing steel behavior is defined as an elasto-plastic constitutive law as,

$$f_s = E_s \varepsilon_s \text{ if } 0 \leqslant \varepsilon_s \leqslant \varepsilon_y \tag{14}$$

$$f_s = f_y \text{ if } \varepsilon_s \geqslant \varepsilon_y \tag{15}$$

where f_s, ε_s are the steel stress and strain, respectively; $E_s = 200$ [GPa] is the elastic modulus of steel; and f_y is the yield steel stress.

2.3. Shear strength determination

The model, given a certain principal direction angle, can determine the entire shear force versus shear displacement curve thought an incremental analysis (incremental values of γ_{Lt}). Thus, the shear strength is defined as the maximum shear force. This is because, for a shear strain value γ_{Lt}, the model iterates over the principal compressive strain deformation ε_d until it complies with the system vertical equilibrium ($\sigma_L = \frac{N}{A}$, where N is the applied vertical load and A is the transverse area of the wall).

2.4. Modifications

The principal direction angle used by Kassem and Elsheikh [9] presents problems in those cases where there is no web reinforcement (and no axial load) because the angle expression that uses a term $(\rho_L/f_L)/(\rho_t/f_t)^{0.1}$ becomes indeterminate (steel stress is assumed yielding). Massone and Ulloa [10] developed a new principal direction angle, based on experimentally validated strain expressions for walls [15]. In this work, an underestimation of shear capacity for short walls is observed as the amount of boundary reinforcement increases. With this motivation, Massone and Álvarez [11] incorporate the boundary reinforcement in the equilibrium expression that characterizes the

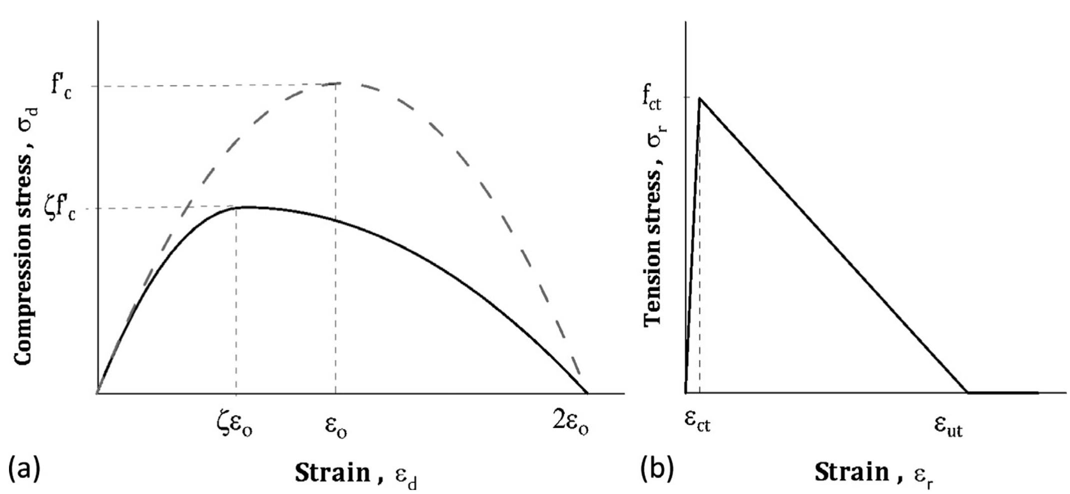

Fig. 2. Concrete constitutive laws – (a) in compression [13], and (b) in tension [14].

longitudinal stress of the panel element for the case of corbels, as

$$\sigma_L = \sigma_d \cos^2\alpha + \sigma_r \sin^2\alpha + \rho_L f_L + \beta\rho_b f_b \tag{16}$$

where f_b, ρ_b are the main or boundary (located at element edges) reinforcement steel stress and ratio in the direction L, respectively (this differs from the distributed longitudinal reinforcement located in the element web, designated as f_L and); and $\beta = 0.3$ is an efficiency factor of the main reinforcement.

The previous model formulation applied to walls [10] did not incorporate the transverse reinforcement in the fixed-angle formulation, given that the amount of reinforcement was relatively low with little impact in the strength prediction. Massone and Orrego [12] applied the fixed-angle panel model for reinforced concrete beam-column joint. Such structural elements are characterized by having large amounts of transverse reinforcement in comparison with short walls (the amount of transverse reinforcement reaches values of 3% in the studied database, which is not observed in short walls). Thus, in order to adjust the model to this structural system, the transverse reinforcement is incorporated directly into the model formulation. For this, a contribution based on equilibrium related to the transverse reinforcement is incorporated in the concrete tensile capacity according to the work by Wang et al. [16], as

$$f'_{ct} = 0.4\sqrt{f'_c\,[\mathrm{MPa}]} + \rho_{sh} f_{yh} \cos^2\alpha \tag{17}$$

where ρ_{sh} and f_{yh} are the transversal steel ratio and yield stress, respectively.

In addition, Massone and Orrego [12] incorporated the confinement effect caused by beams and columns adjacent to the joint. With this objective, the equations of horizontal and vertical strains (ε_t, ε_L) [15] are modified by applying a factor that considers the strain decrease due to confinement as $\varepsilon_t^{mod} = \varepsilon_t(1-\lambda_t)$ and $\varepsilon_L^{mod} = \varepsilon_L(1-\lambda_L)$, respectively. As defined, the factors λ_t and λ_L vary between 0 and 1, where 0 means no effect and 1 means full constrain that reduces the respective strain to zero. The factors were optimized such that the best strength predictions are obtained, distinguishing between interior and exterior joints, since confinement is commonly higher in the first case. Thus, with the new strain expressions the principal direction angle is defined as (with a similar procedure as described in Section 4.2),

Exterior joint

$$\alpha = 17.6\left(\frac{H_w}{L_w} + 0.5\right)^{-0.02}\left(\frac{N}{f'_c t_w L_w} + 0.1\right)^{-0.46} \tag{18}$$

Interior joint

$$\alpha = 19.8\left(\frac{H_w}{L_w} + 0.5\right)^{-0.04}\left(\frac{N}{f'_c t_w L_w} + 0.1\right)^{-0.43} \tag{19}$$

3. Database description

A database of tests from research projects in the literature is compiled. 635 tests are considered, corresponding to 252 of short walls, 182 of deep beams, 109 of corbels, and 92 of beam-column joints. The detailed description of the database can be found as a supplementary material, as well as in Melo [17], and partially in Massone and Ulloa for walls specimens [10], Massone and Alvarez for corbels specimens [11], and Massone and Orrego for beam-column joint specimens [12].

The database of 252 short walls consists of 85% of cantilever specimens and 15% of double curvature tests. The boundary reinforcement ratio varies from 0.7% to 11%. The vertical and horizontal reinforcement ratio vary between 0% and 3.7%, while the yield stress of all reinforcing bars is between 209 [MPa] and 624 [MPa]. The compressive strength of concrete varies from 12.4 [MPa] to 63.4 [MPa]. The axial load, applied only in some cases, reaches a maximum value of $0.27 f'_c L_w t_w$.

The database of 182 tests of deep beams consists of 150 cases with transverse reinforcement. The vertical reinforcement (transversal) ratio ranges from 0% to 2.7% and the horizontal (longitudinal) reinforcement varies between 0% and 3.2%. The reinforcement ratio for positive bending ranges between 0.5% and 2.6%, while the reinforcement for negative bending ranges from 0% to 0.9%. The yield stress of the bars ranges from 287 [MPa] to 804 [MPa]. The compressive strength of concrete ranges from 16 [MPa] to 86 [MPa]. The aspect ratio a/d ranges from 0.27 to 2.7.

The 109 corbel tests lack of transverse reinforcement and 51% of the tests do not have secondary web reinforcement. All tests were performed in the absence of axial load. The web longitudinal reinforcement ratio goes from 0% to 1.6%, whereas the main tensile reinforcement ratio goes from 0.29% to 4.9%. The effective aspect ratio a/d ranges from 0.15 to 1.01. The yield stress of steel bars varies between 303 [MPa] and 558 [MPa]. The compressive strength of concrete ranges from 15 [MPa] to 105 [MPa].

The database of beam-column joints correspond to 92 tests, with 54 specimens that are external joints and 38 that are internal joints. The compressive strength of concrete varies from 22.1 [MPa] to 92.4 [MPa]. The longitudinal reinforcement steel ratio ranges from 0% to 4%, the boundary steel reinforcement ratio varies between 0.5% and 3.5% and the transversal reinforcement steel ratio between 0% and 3%. The yield stress of the longitudinal and boundary reinforcing steel varies between 280 [MPa] and 644 [MPa], and the transverse reinforcing steel between 235 [MPa] and 1320 [MPa]. The compression axial tension ranges from 0 to $0.75 f'_c$.

In order to compare the shear capacity predicted by the model with the flexural capacity, models are implemented following the recommendations of ACI 318 by means of a sectional analysis [18].

4. Closed-form model development

4.1. General model for all four structural systems

In this section, the model is generalized and applied to four structural systems. The model can be used for any reinforced concrete panel controlled by shear, and an analogy between the common structural types is included for clarity. This analogy is based on relating the height H_w and the effective length d_w of the wall element with the dimensions of the 3 remaining structural systems, which is schematized in Fig. 3. For the case of deep beams, the panel that characterizes the shear capacity of the element is defined by the point of application of the load and support. Thus, such distance of the beam is similar to the height of the short wall. As for corbels, the simile with short walls is obtained by rotating the structural element by 90°. Thus, the corbel is represented as a small cantilevered wall of low aspect ratio. Finally, for beam-column joints the geometry is similar to the case of short walls. It is necessary to emphasize that, for deep beams and corbels, H_w is defined discounting the load plate width, as proposed by [19], since the load plate limits the expansion of strains in the surroundings. On the other hand, for deep beams, corbels and beam-column joints, it is assumed that d_w corresponds to the length between the edge of the structural element (most compressed zone) and the tensile boundary reinforcement.

4.2. Recalibration of the principal direction angle

Using the database for short walls, deep beams and corbels, a new general principal direction angle is calibrated for these three structural systems. For this purpose, the same method previously applied (e.g. [10,11,12]) is used to estimate the angle of the principal direction at the cracking level of the structural element. Although there are two

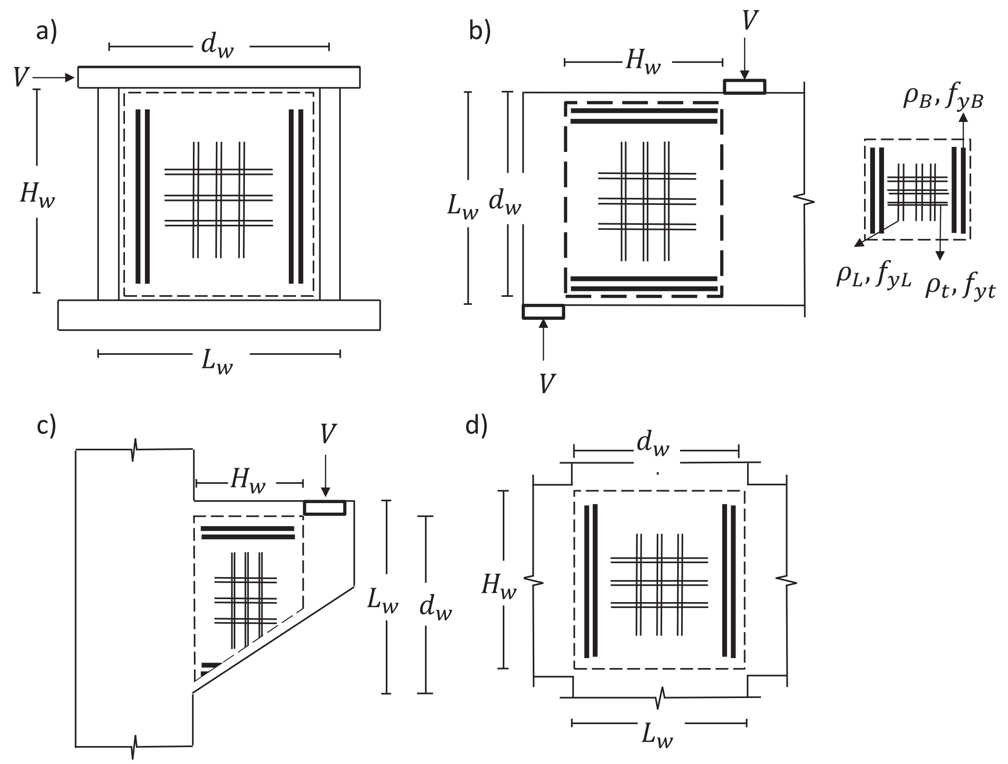

Fig. 3. Element analogy – (a) short wall, (b) deep beam, (c) corbel and (d) beam-column joint.

different approaches for the crack direction (rotating-angle and fixed-angle approach), there is experimental evidence showing that the direction of principal strain tends to keep a preferred angle once the cracks in concrete appear (e.g., short walls [9]). When several cracks occur in concrete the compression strut develops, so that the angle of compression strut is stabilized for greater drifts or deformations. The beginning of the cracking is characterized by the tensile capacity of concrete ($\sigma_r = f'_{ct}$), whose state is used to determine the fix angle α. In this case, the effect of the transverse reinforcement defined in Eq. (17) is considered. Then, at concrete cracking, and assuming a certain drift γ_{Lt}, it is possible to calculate the longitudinal (ε_L) and transverse (ε_t) deformation of the structural element by means of calibrated expressions [13], which allows to calculate the principal strain direction according to $\alpha = \tan^{-1}(-(\frac{\varepsilon_t - \varepsilon_L}{\gamma_{Lt}}) + \sqrt{(\frac{\varepsilon_t - \varepsilon_L}{\gamma_{Lt}})^2 + 1})$. With this angle, the tensile strain is obtained as $\varepsilon_r = \frac{\gamma_{Lt}\tan\alpha}{2} + \varepsilon_t$, which must be equal than the cracking strain. This analysis is performed until cracking is reached by imposing an incremental drift $\Delta\gamma_{Lt}$.

Thus, a series of values of principal direction angles at cracking, for different structural systems and geometric and material parameters, are obtained. With these results, and defining the most relevant parameters, a calibration using the least squares method is performed to obtain an expression for the principal direction angle. Thus, calibrated expressions for elements with simple and double curvature are shown below:

Simple curvature(short walls, deep beams, corbels)

$$\alpha = 13.9\left(\frac{H_w}{L_w} + 0.5\right)^{-0.13}\left(\frac{N}{f'_c t_w L_w} + 0.1\right)^{-0.67} \tag{20}$$

Double curvature(short walls)

$$\alpha = 9.81\left(\frac{H_w}{L_w} + 0.5\right)^{-0.08}\left(\frac{N}{f'_c t_w L_w} + 0.1\right)^{-0.78} \tag{21}$$

The expressions for beam-column joints are still those determined by Massone and Orrego [12] (Eqs. (18) and (19)), since these incorporate additionally the confining effect.

4.3. Shear strength for different limit states

In order to obtain the shear capacity of the structural elements, instead of performing an incremental analysis, the strain values corresponding to the four possible maximum stresses or limit states are used. These peak strength values correspond to cases where one of the following is reached: the tensile or compressive capacity of concrete or the yielding of longitudinal or boundary reinforcement. The strain and stress associated with each maximum is determined with the respective material constitutive laws. Thus, the strains and the stresses are defined as shown in Table 1. With this incorporation, instead of fixing the drift of the element, each strain value is imposed. The modification applied in the incremental model is shown in the schematic flow diagram presented in Fig. 4, where the step corresponding to the incremental analysis, which assumes small drift increments, is replaced by analyzing the four limit states.

When calculating the shear strength associated to the four limit states, by means of a numerical method that iterates in the strains of the panel element, the shear capacity of the structural element is obtained as the greatest of the four possible values. The points of maximum capacity for two tests of short walls from the database, one for an element that fails in compression and another that reaches yielding of the reinforcement, are presented in Fig. 5. In this figure, the shear force versus shear strain curve is presented, which is calculated by incremental analysis (requires iteration of the equilibrium equation) and the method proposed for both specimens (not incremental, but requires

Table 1
Strains and stresses associates to all 4 limit states.

Limit state	Strain	Stress
Concrete compression	$\varepsilon_d^* = -\xi\varepsilon_o$	$\sigma_d^* = -\xi f'_c$
Concrete tension	$\varepsilon_r^* = f'_{ct}/E_c$	$\sigma_r^* = f'_{ct}$
Longitudinal reinforcement yielding	$\varepsilon_L^* = f_{yL}/E_S$	$\sigma_L^* = f_{yL}$
Main reinforcement yielding	$\varepsilon_L^* = f_{yb}/E_S$	$\sigma_L^* = f_{yb}$

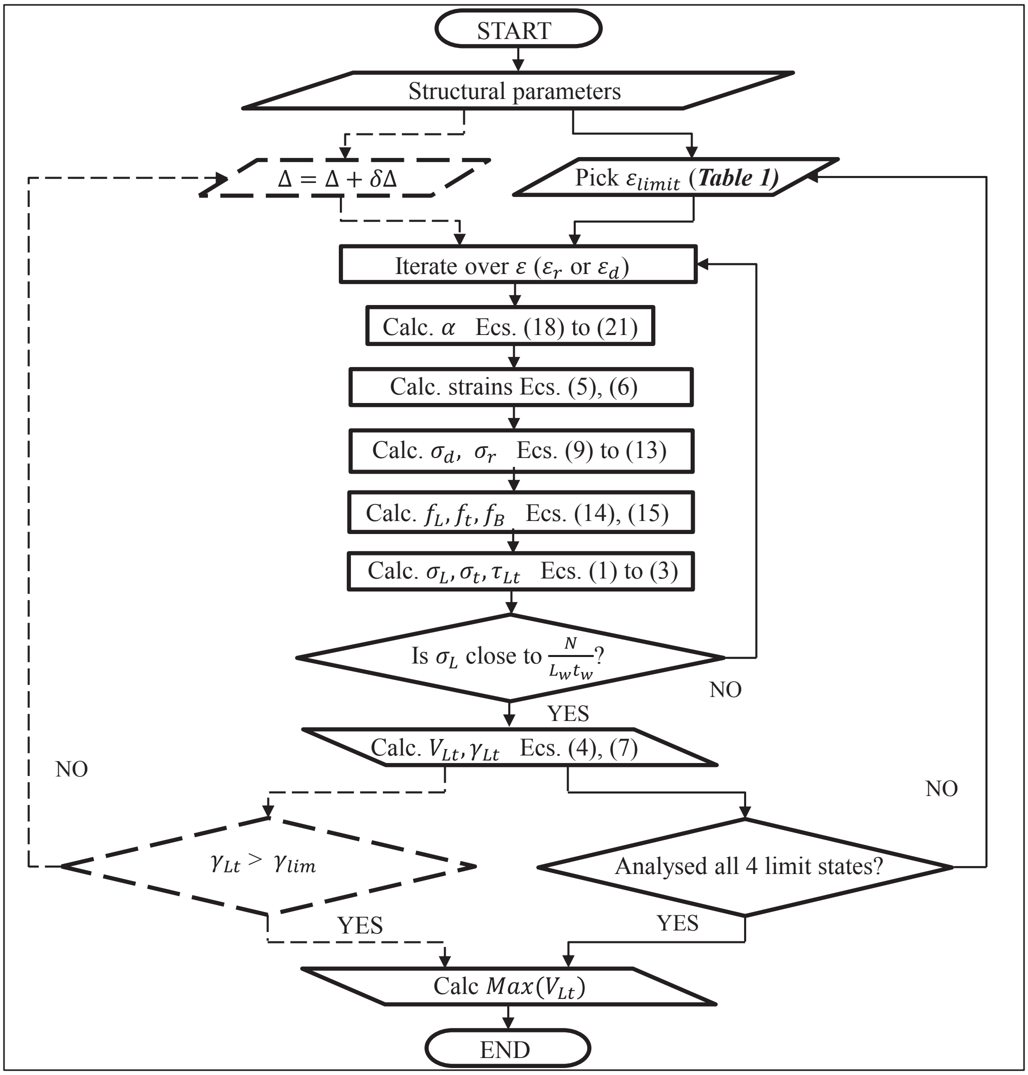

Fig. 4. Flow chart of incremental model (dashed line) and 4-limit state model (solid line).

iteration of the equilibrium equation). Thus, the points in the figure correspond to the different limit states, which guarantee that this method is capable of capturing the maximum capacity. As can be seen in the figure, not all limit states are reached in each test. Even though the full model formulation (before achieving the closed-form solution) is capable of estimating the overall shear response, this work focuses on strength prediction. The work by Massone and Ulloa [10] shows comparisons for short walls, where the overall response is well captured,

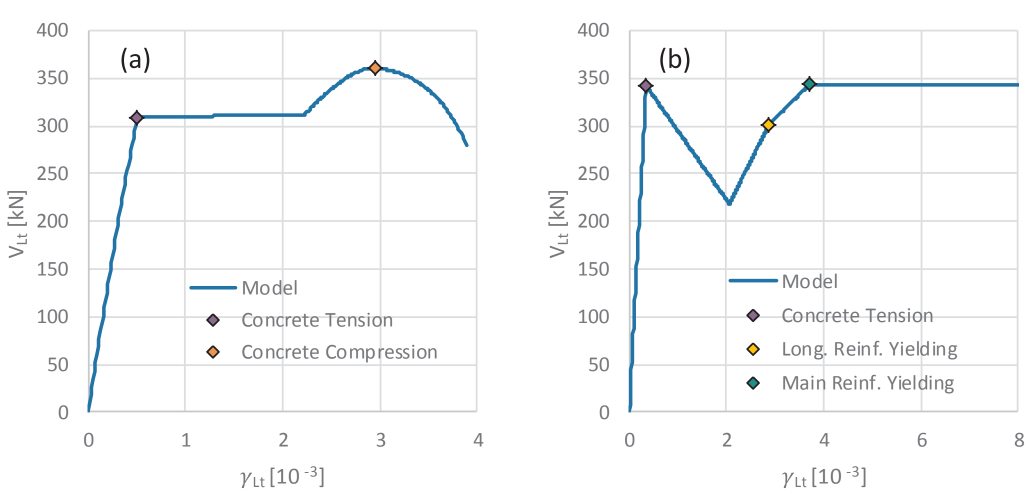

Fig. 5. Estimation of shear capacity for different limit states – (a) specimen reaching capacity due to concrete in compression, and (b) specimen reaching capacity due to yielding of reinforcement.

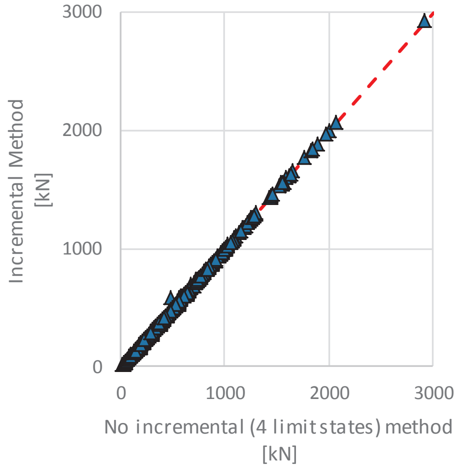

Fig. 6. Shear strength correlation between iterative incremental model and 4-limit state (non-incremental) model.

but more refined material models are required to better resemble the experimental response.

Then, for the database of all four structural systems, the capacity obtained by the iterative model that requires an incremental analysis is compared with the proposed non-incremental method. This comparison is presented in Fig. 6, where it can be seen that the capacity difference predicted by both approaches is minimal, and the data is almost perfectly adjusted to the 45° line. Thus, incorporating the proposed method to the fixed-angle model is beneficial from the computational optimization point of view.

4.4. Strain calibration for closed-form solution

In order to avoid the iterative procedure that involves the calculation of the shear capacity for all limit states, a strain calibration is performed on the model. Thus, the principal tensile or compressive concrete strain (ε_r or ε_d, respectively) is calibrated for each limit state, which would allow a closed-form solution for the model. The principal tensile concrete strain ε_r is calibrated for the limit state associated with concrete compression failure, the principal compression strain ε_d for the limiting state associated with concrete cracking and another expression for the yielding of boundary and web longitudinal reinforcement. For simplicity, for the last two components (yielding of longitudinal reinforcement), a single expression is calibrated, since both components are included similarly in the formulation and material properties are commonly identical.

The calibration is performed as a multiple regression using the least squares method, on 7 variables that describe the strain of the panel element. The used variables are the longitudinal, transversal and boundary reinforcement ($\rho_L f_{yL}/f'_c$, $\rho_t f_{yt}/f'_c$, $\beta\rho_b f_{yb}/f'_c$,), the axial load ($N/f'_c L_w t_w$), the principal strain (or concrete stress) direction angle ($\cos(\alpha)$), the aspect ratio (H_w/L_w) and the compressive strength of concrete (f'_c), which turns out to be the only non-dimensionless variable selected for the analysis. The least squares method is applied to logarithmic expressions that incorporate at most four variables, as shown below:

$$\varepsilon_{r\acute{o}d}(var_1, \ ..., var_n) = C(var_1 + c_1)^{k_1}(var_2 + c_2)^{k_2}...(var_n + c_n)^{k_n} \tag{22}$$

With $n \leqslant 4$, var_i the variable i chosen from the list of 7 parameters, c_i the constant relative to the variable i and C a dimensionless constant.

After obtaining the strain values associated with each limit state, a calibration procedure is implemented. For this, out of the 7 variables presented, those whose impact on the correlation (measured by the coefficient of determination R^2) between the strain obtained by the iterative model and that estimated by the calibration are less relevant, are eliminated, one by one. The results of this procedure are presented in Fig. 7, where the coefficient of determination (R^2) of each limit state (best solution) is shown, according to the variables used for the calibration. From left to right, the first case considers all the variables (that is, none is eliminated) to then eliminate the variable indicated in the figure, and continue eliminating the previous and the indicated variables, until the last case. This is done for the calibration associated with the tensile limit state of the concrete (Fig. 7a), the concrete compression limit state (Fig. 7b) and the vertical reinforcement yielding limit state (Fig. 7c). One of the first variables that is discarded for all limit states is the aspect ratio, which shows almost no reduction on accuracy once is removed. As can be seen in the figure, the principal direction angle has a relevant correlation for the 3 cases, as well as, the reinforcement and the axial load. The aspect ratio is the parameter with the least influence in the correlation, followed by the concrete compressive strength. The latter is only relevant for the case of tension concrete.

Once the calibrated expressions that avoid the iterative process are obtained, it is necessary to provide conditions that allow distinguishing

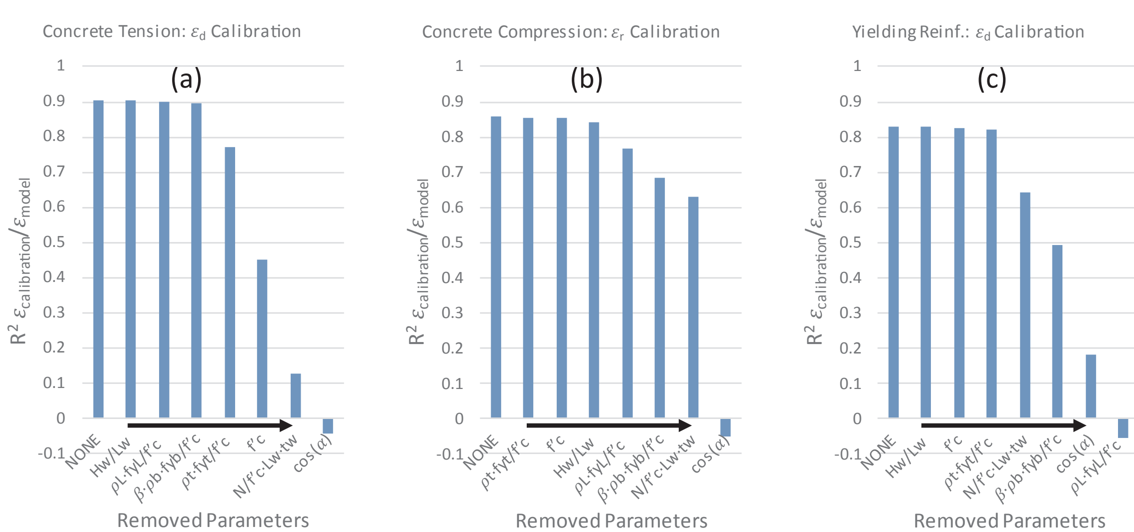

Fig. 7. Correlation coefficient of strain calibration for different number of variables – (a) concrete in tension, (b) concrete in compression, and (c) yielding of reinforcement.

the different limit states that actually develop for a structural element, and therefore comply with the vertical equilibrium equation. Not all limit states can be reached for every case. One way to avoid this problem is to determine if the capacity associated with the diagonal compression limit state is reached (for a shear drift γ_{Lt_c}) before the yielding of the distributed longitudinal or boundary reinforcement (for a shear drift $\gamma_{Lt_{f_{yL}}}$ or $\gamma_{Lt_{f_{yb}}}$). For the range of drift to which the compression and reinforcement yielding occur (0.1–0.3%) the contribution of the concrete tension is negligible. Then, if the concrete compression capacity is reached, the tension of the longitudinal and boundary reinforcement cannot increase because the vertical equilibrium must be maintained. Thus, if the drift related to the reinforcement yielding is greater than the drift associate to the maximum compression, the points associated to yielding must be omitted, since they do not comply with the equilibrium (Eq. (23)). Conversely, if yielding of both reinforcements develops, the strength of concrete in compression cannot be reached later. Thus, if the drifts values associate to yielding of reinforcement are less than the drift for the maximum compression, the last must be omitted (Eq. (24)). Thus, based on the formulation of the panel model, the following conditions are imposed:

$$If \begin{Bmatrix} \gamma_{Lt_c} \leqslant \gamma_{Lt_{f_{yL}}} \\ or \\ \gamma_{Lt_c} \leqslant \gamma_{Lt_{f_{yb}}} \end{Bmatrix} \Rightarrow \begin{Bmatrix} V_{Lt_{f_{yL}}} \\ and \\ V_{Lt_{f_{yb}}} \end{Bmatrix} cannot\ be\ reached \tag{23}$$

$$If \begin{Bmatrix} \gamma_{Lt_c} \geqslant \gamma_{Lt_{f_{yL}}} \\ and \\ \gamma_{Lt_c} \geqslant \gamma_{Lt_{f_{yb}}} \end{Bmatrix} \Rightarrow V_{Lt_c}\ cannot\ be\ reached \tag{24}$$

where γ_{Lt_c}, V_{Lt_c}, $\gamma_{Lt_{f_{yL}}}$, $V_{Lt_{f_{yL}}}$, $\gamma_{Lt_{f_{yb}}}$ and $V_{Lt_{f_{yb}}}$ correspond to the drift and shear force associated to the limit state of compression, yielding of longitudinal and boundary reinforcement, respectively.

Taking into consideration the limit state that can be achieved, closed-form models are generated by selecting a calibrated expression, with four or less variables, for each limit state case. Despite the fact that Fig. 7 provides relevant information regarding which parameters to consider for a good estimation of the strain, it is necessary to verify that such good correlation is transferred to the estimation of the capacity. Thus, the generated closed-form models are statistically evaluated by means of the average of the estimated capacity over the experimental ratio (V_{model}/V_{test}) and its coefficient of variation COV, with the objective of determining the one that presents less scatter (lower COV). The study is done by generating closed-form models that use all possible combinations of expressions of four or fewer parameters (a total of 125 models). In Fig. 8 the result of this analysis is plotted where, for each limit state, and in a decreasing order of number of parameters used in the expression, the coefficient of variation of the model with best correlation is shown. Fig. 8a shows the results for the tensile limit state in concrete, varying the number of parameters from 4 to 0 (left to right), where the order of parameters is the same used for Fig. 7. Similarly, Fig. 8b shows the results for the compression limit state in the concrete (4–0 parameters), and Fig. 8c the case of yielding of the vertical reinforcement. Thus, it is observed that, while for concrete compression and reinforcement yielding the error increases in the closed-form model of better performance, as the number of expression parameters decreases, this does not occur for the tension of the concrete; since the model that shows lower COV is one that integrates 2 parameters in the expression. This shows that increasing the number of calibration variables made for strain does not directly imply an improvement in the ability of the model to predict the capacity of the structural element, which is explained by the imposed conditions of Eqs. (23) and (24). Finally, from this figure it is clear that the closed-form model with the least error considers 4 parameters for the expression of reinforcement yielding, 4 for compression and 2 for tension of concrete. The expressions related to the aforementioned parameters are shown below for each limit state, where the three expressions include the axial load and the principal direction angle in its formulation. Eqs. (25)–(27) provide the calibration of a strain variable for each limit state (tension, compression or reinforcement yielding). In the case of principal compressive strain (ε_d), which is selected for Eqs. (25) and (27), there is direct correlation to the level of axial load, which is consistent with the longitudinal equilibrium (Eq. (16)), such that the larger the axial load the larger the compressive strain. Moreover, the exponents for the axial load are similar for both equations, which is also observed with the principal direction angle exponent. On the other hand, Eq. (26) for the tensile principal direction (ε_r) reduces its magnitude with the increase of axial load. In the case of longitudinal reinforcement (distributed and boundary), which appears in the longitudinal equilibrium equation, is also relevant for Eqs. (26) and (27), with larger compressive strains (Eq. (27)) and smaller tensile strains (Eq. (26)) for larger reinforcement amount, which is also consistent with the longitudinal equilibrium (Eq. (16)).

Tension

$$\varepsilon_d = -1.29\text{x}10^{-3}(\cos\alpha)^{-2.56}\left(\frac{N}{f'_c A_g} + 0.1\right)^{1.40} \tag{25}$$

Compression

$$\varepsilon_r = 3.61 \times 10^{-4}\left(\frac{\rho_L f_{yL}}{f'_c} + 0.05\right)^{-0.59}\left(\frac{\beta\rho_b f_{yb}}{f'_c} + 0.05\right)^{-0.60}(\cos\alpha)^{3.46}\left(\frac{N}{f'_c A_g} + 0.1\right)^{-0.86} \tag{26}$$

Reinf. yielding

$$\varepsilon_d = -0.635\left(\frac{\rho_L f_{yL}}{f'_c} + 0.05\right)^{1.24}\left(\frac{\beta\rho_b f_{yb}}{f'_c} + 0.05\right)^{1.22}(\cos\alpha)^{-2.45}\left(\frac{N}{f'_c A_g} + 0.1\right)^{1.36} \tag{27}$$

In this way, the analysis of the closed-form model for shear strength estimate requires the evaluation of compatibility equations, constitutive law and equilibrium for the 4 limit states of the structural element, which is described in the flow chart of Fig. 9.

With this methodology, the performance of the closed-form model ($V_{closed-form}$) developed is compared with the iterative model ($V_{iterative}$) and the experimental capacities (V_{test}). For this, the ratios $V_{closed-form}/V_{iterative}$, $V_{closed-form}/V_{test}$ and $V_{iterative}/V_{test}$ with respect to the database are evaluated statistically by the average and coefficient of variation (COV), in order to verify the correct performance of the closed-form model. The results of the models are shown in Figs. 10 and 11. The relationship between $V_{closed-form}$ and $V_{iterative}$ is shown in Fig. 10, but in terms of tension ($\tau_{Lt} = V/t_w d_w$), where the estimated data for the entire database (all four structural elements) are kept close to the axis at 45°, which indicates an adequate correlation between both models. The response of the ratios $V_{closed-form}/V_{test}$ and $V_{iterative}/V_{test}$ is shown in Fig. 11a and b, respectively, where both models have similar averages (1.0 and 0.98, for closed-form and iterative model, respectively) and COVs (0.25 and 0.23, for closed-form and iterative model, respectively) with respect to the experimental capacities for all specimens. In addition, the predicted failure modes (bending or shear) are maintained from the iterative model to the closed-form model, which guarantees that the incorporation of the calibrated expressions does not affect the physics of the phenomenon. The results indicate good correlation between the model and the test results with an average close to 1 and moderate COV. However, there are few cases (~1%) that predict shear strength

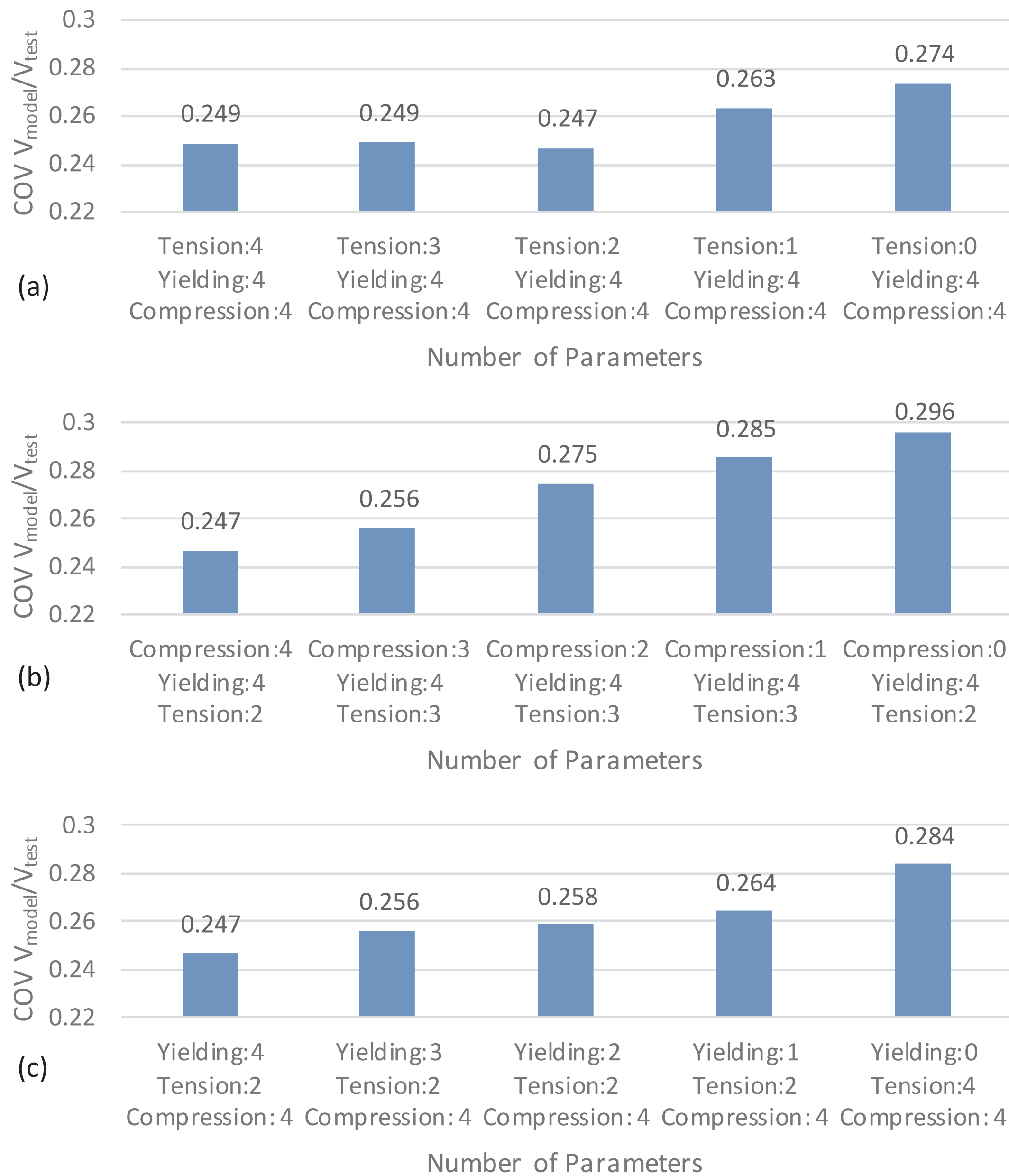

Fig. 8. Scatter of shear strength ratio for strain calibration based on different number of variables – (a) concrete in tension, (b) concrete in compression, and (c) yielding of reinforcement.

that are 50% or larger than observed, which are unconservative and might not be covered by safety coefficients. Considering the large database, it represents a small defective fraction.

4.5. Comparison with ACI 318 and AASHTO

The experimental capacity of the 4 structural systems compiled is compared with the expressions defined in the AASHTO [20] and ACI 318 [18]. In the case of ACI 318, an earlier version is used for deep beams [3].

For short walls, the ACI 318 standard superimposes the contribution of concrete and horizontal reinforcement steel to the shear strength. The contribution of concrete (V_c) depends on the aspect ratio of the wall. As for steel, only the contribution of the distributed horizontal reinforcement (V_s) is considered, assuming that the steel bars are yielding. Thus, the capacity (V_n) is defined by

$$V_n = V_c + V_s \leqslant 0.83\sqrt{f_c'}A_w \tag{28}$$

$$V_c = \alpha_c\sqrt{f_c'}A_w \tag{29}$$

$$V_s = \rho_t f_{yt} A_w \tag{30}$$

where A_w is the gross area of the cross section, ρ_t is the transverse steel ratio, and f_{yt} is the yield stress of transverse steel reinforcement. The coefficient α_c is a function of the aspect ratio, and takes value of 0.25 for $H_w/L_w < 1.5$, and 0.17 for $H_w/L_w > 2$, and is interpolated linearly for intermediate values.

Regarding deep beams, the ACI 318 characterizes them with an effective length over an effective height ratio less than 1.25 for simply supported beams, and less than 2.5 for continuous beams. Thus, for the study of this section, the comparison of the closed-form model and ACI 318 is carried out considering only specimens that comply with these limits. In this case, and as same as for short walls, shear strength

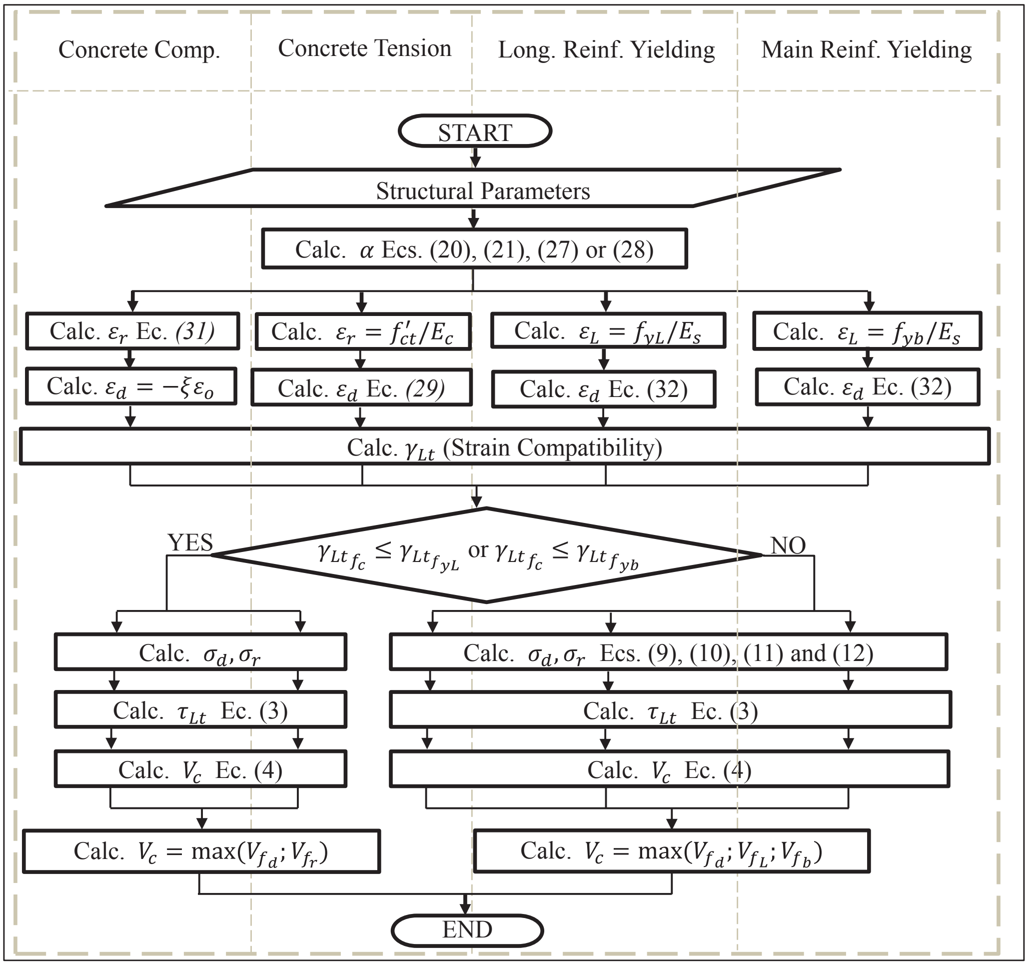

Fig. 9. Flow chart of the shear strength closed-form model.

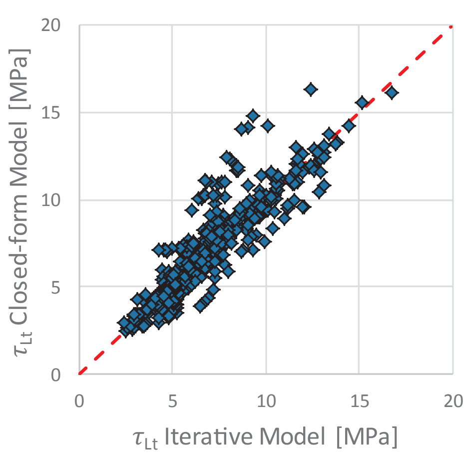

Fig. 10. Comparison between the shear stress estimates for the closed-form ($\tau_{Lt,closed-form}$) and iterative ($\tau_{Lt,iterative}$) models for all 4 structural systems.

considers superimposing the contribution of reinforcement and concrete, as

$$V_n = V_c + V_s \leqslant \left\{ \begin{matrix} 0.66\sqrt{f'_c}\, b_w d \;\text{if}\; \frac{l_n}{d} < 2 \\ 0.056\left(10 + \frac{l_n}{d}\right)\sqrt{f'_c}\, b_w d \;\text{if}\; 2 \leqslant \frac{l_n}{d} < 5 \end{matrix} \right\} \tag{31}$$

$$V_c = \left(3.5 - \frac{2.5M_u}{V_u d}\right)\left(\sqrt{f'_c} + 120\rho_w \frac{V_u d}{M_u}\right)\frac{b_w d}{7} < 0.5\sqrt{f'_c}\, b_w d \tag{32}$$

$$\left(3.5 - 2.5\frac{M_u}{V_u d}\right) < 2.5 \tag{33}$$

$$V_s = \left[\frac{A_v}{s}\left(\frac{1 + \frac{l_n}{d}}{12}\right) + \frac{A_{vh}}{s_2}\left(\frac{11 - \frac{l_n}{d}}{12}\right)\right] f_y d \tag{34}$$

where M_u and V_u are the maximum moment and shear in the critical section of the element, respectively, ρ_w is the main reinforcement ratio, f_{yh} is the yield of the horizontal reinforcement steel, A_v and A_{vh} are the area of the vertical and horizontal reinforcement bars, respectively, s and s_2 are the spacing of the vertical and horizontal reinforcement, respectively, l_n is the distance between the faces of support points, b_w is the thickness of the beam, and d represents the effective height of the beam.

For reinforced concrete corbels with an aspect ratio less than 1, the ACI 318 presents a special section for the estimation of the shear capacity based on a shear friction model. The model assumes that both the main and secondary steel that cross the failure plane (perpendicular to the reinforcement) are yielding. Thus, the capacity is defined as,

$$V_n = \mu(\rho_f f_{yf} + \rho_h f_{yh}) bd \leqslant \min\left\{ \begin{matrix} 0.2 f'_c \\ 11\ [\text{MPa}] \\ 3.3\ [\text{MPa}] + 0.08 f'_c \end{matrix} \right\} bd \tag{35}$$

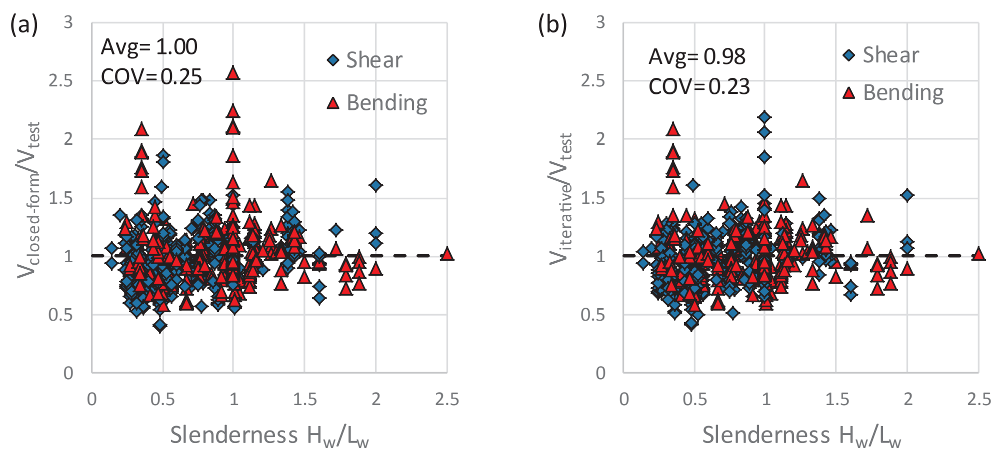

Fig. 11. Strength ratio $V_{closed-form}/V_{test}$ and $V_{iterative}/V_{test}$ for predicted shear and flexural failure for all 4 structural systems.

where μ is the coefficient of friction, equal to 1.4 for monolithic constructions of normal weight concrete, ρ_f and ρ_h are the main and secondary reinforcement ratio, respectively, f_{yf} and f_{yh} are the yield stress of the main and secondary steel, respectively.

In the case of beam-column joints, according to ACI 318, the capacity is obtained depending on the level of confinement as,

$$V_n = \begin{cases} (a)\ Confined\ in\ 4\ faces & 1.7\sqrt{f_c'}A_j \\ (b)\ Confined\ in\ 3\ faces\ or\ 2\ opposite\ faces & 1.2\sqrt{f_c'}A_j \\ (c)\ Other\ cases & 1.0\sqrt{f_c'}A_j \end{cases} \quad (36)$$

where A_j represents the effective area of the joint. Out of the three forms exposed in Eq. (36) to calculate the shear capacity, case (b) is used for internal joints that have three or two opposite beams that converge to the node, and that cover more than three quarters of the face of the column, and case (c) is used if such beams cover less than three quarters of the column face or if the joint is external. Finally, case (a) is used for internal joints that meet the condition of confinement on all four sides of the column.

In the case of AASHTO [20], the shear strength expression is consistent with the approach developed by Collins et al. [4]. The design approach uses a simplified version of the MCFT [5] separating the shear strength in two components, one associated to the concrete strength and another to the transversal reinforcement. In the case of concrete, instead of using a constant strength capacity for concrete, as ACI 318 considers in most models, the strength reduces with the longitudinal strain in the element section, among other factors. The shear strength of concrete is defined as,

$$V_c = \beta\sqrt{f_c'}\,b_w d_v \leqslant 0.25 f_c' b_w d_v \quad (37)$$

where β is a reduction factor that account for longitudinal tensile strain in the main reinforcement of the section (ε_s), with $\beta = 0.4/(1 + 750\varepsilon_s)$ for elements with minimum shear reinforcement and $\beta = 0.4/(1 + 750\varepsilon_s)\cdot 1.3/(1 + s_{xe})$ for other cases; s_{xe} (m) is a crack spacing parameter; d_v is the effective shear depth (moment arm between the compressive force and tensile force of main reinforcement); $\varepsilon_s = (M_u/d_v - 0.5N_u + V_u)/(E_sA_s)$ is the longitudinal strain of the main reinforcement for cases without pre-stressing forces; M_u, N_u, V_u are the moment, axial load (compression is positive) and shear actions in the section; and E_sA_s is the main reinforcement stiffness.

In the case of transversal reinforcement, the contribution is defined as,

$$V_s = A_v f_y d_v cot\theta/s \quad (38)$$

where $A_v f_y d_v/s$ is taken in this work as the total force that can be developed in the horizontal reinforcement, and $\theta(°) = 29 + 3500\varepsilon_s$.

The performance shown by the code shear strength equations and the proposed closed-form model is compared for all four structural systems. This is done by statistically evaluating the performance of the average and coefficient of variation (COV) of the ratio V_{model}/V_{test} with respect to the database. In addition, the sensitivity is analyzed with respect to all 7 parameters that characterize the shear capacity, such as the slenderness H_w/L_w, the axial load $N/(f_c'A_g)$, the longitudinal reinforcement $\rho_L f_{yL}$, the transverse reinforcement $\rho_t f_{yt}$, the boundary reinforcement $\rho_b f_{yb}$, the compressive strength of concrete f_c', and the principal direction angle α. The results are presented in Figs. 12–15, where for each structural system (Fig. 12 for walls, Fig. 13 for deep beams, Fig. 14 for corbels and Fig. 15 for beam-column joints), the ratio between the predicted capacity (ACI 318, AASHTO and the closed-form model) and the experimental capacity is shown, only for those elements whose failure is predicted as shear. In each figure the results are shown for the parameter in the horizontal axis that shows the lowest (Figs. 12a–15a) and highest (Figs. 12b–15b) dependence of the proposed model to any of those previously declared variables (7 parameters) by means of its trend line (also shown for the ACI 318 and AASHTO expressions). This is done in order to compare the sensitivity shown by the closed-form model with respect to its parameters, where greater variation (away from 1) of the trend line represents greater sensitivity, implying that the model is less able to capture the associated parameter in its formulation. For the analysis, a subset of the database is used to comply with limitations in ACI 318 expressions. As shown in Figs. 12–15, it is concluded that in almost all cases, there is little dependence on the closed-form model to the principal direction angle, while the greater dependence is different depending on the structural element, and in general is associated to some specimens with extreme parameter values that accentuate an apparent dependency. Similarly, the AASHTO expression shows little dependency to the parameters under analysis, with comparable trends as the proposed model, except for beam-column joints where there is dependency to the axial load. The ACI 318, on the other hand, shows significant dependency to some of the described parameters, such as the axial load in beam-column joints (Fig. 15a), since the model does not consider this effect.

Table 2 shows the statistical results that characterize the performance of the proposed model, the AASHTO and the ACI 318 for each of the 4 structural systems, separated by predicted failure mode. Considering that the ACI 318 shear strength predictions tend to be conservative a larger number of tests are predicted with shear failure with this model than with the proposed model. This table shows that, although the performance shown by the predicted flexural cases is similar for all models, the tests predicted to fail in shear by the ACI 318 code equations show a very conservative estimate. The ACI 318 presents its best performance for beam-column joints, with an average underestimation of 20% for shear and a COV of 0.24. On the other hand, the

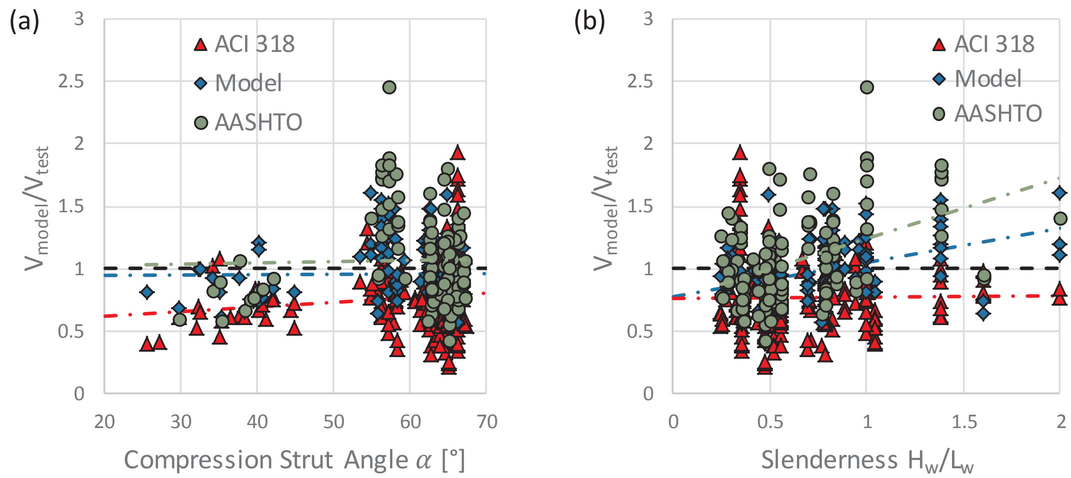

Fig. 12. Sensitivity analysis for short walls – (a) less sensitive parameter, and (b) most sensitive parameter for the proposed model.

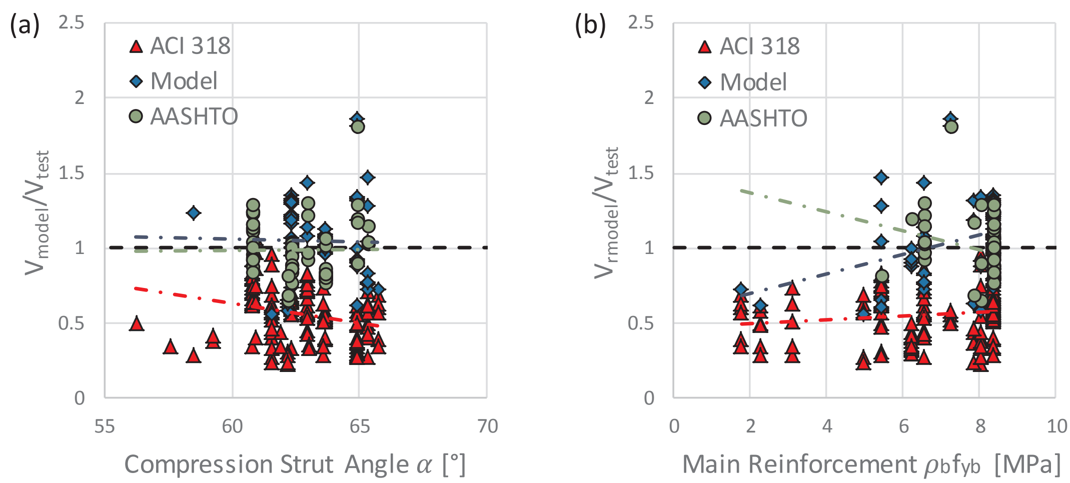

Fig. 13. Sensitivity analysis for deep beams – (a) less sensitive parameter, and (b) most sensitive parameter for the proposed model.

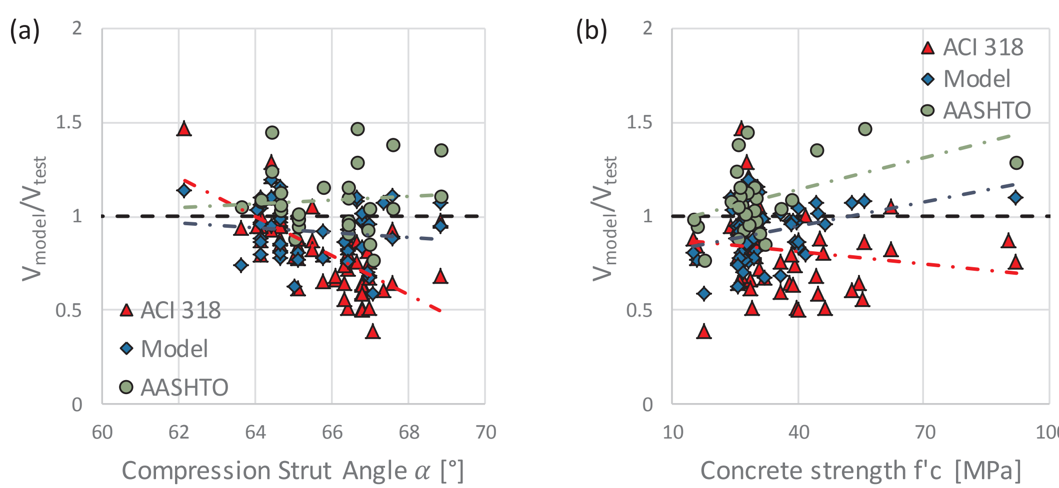

Fig. 14. Sensitivity analysis for corbels – (a) less sensitive parameter, and (b) most sensitive parameter for the proposed model.

deep beams present the worst performance, with average and COV for shear of 0.55 and 0.32. The proposed model shows a similar and good performance for all four structural systems, with strength ratio averages that deviate 5% at most for cases that fail in shear. In the case of AASHTO, the results are as good as the one from the proposed model, with strength ratio averages that deviate 15% at most (shear failure). In addition, the proposed model and AASHTO have relatively low COVs compared to the ACI 318. When all specimens that fail in shear (all 4 element types with reduced database) are considered, the average and COV estimates yield values of 0.99 and 0.23, respectively, for the proposed model, and 1.03 and 0.28, respectively, for the AASHTO expression. Thus, the proposed model shows good agreement with the

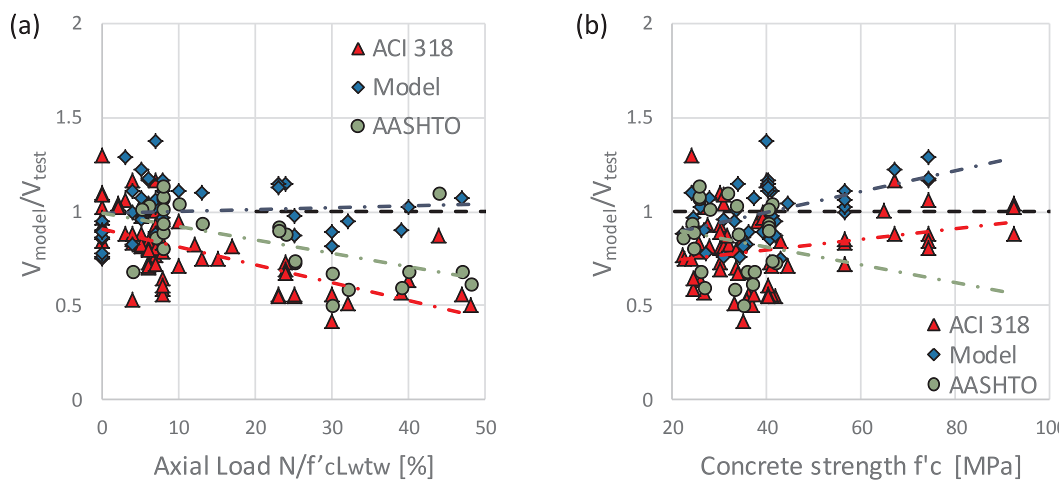

Fig. 15. Sensitivity analysis for beam-column joints – (a) less sensitive parameter, and (b) most sensitive parameter for the proposed model.

Table 2

Statistical analysis of strength estimate ratio for the proposed model, AASHTO and ACI 318 equations for all 4 structural systems.

Case		Short walls			Deep beams			Corbels			Beam-column joints		
		Prop. Model	AASHTO	ACI 318	Prop. Model	AASHTO	ACI 318	Prop. Model	AASHTO	ACI 318	Prop. Model	AASHTO	ACI 318
All	Avg	1.01	1.10	0.81	1.04	1.02	0.58	1.00	1.10	0.84	1.01	0.99	0.83
	COV	0.26	0.30	0.34	0.30	0.31	0.33	0.15	0.14	0.24	0.16	0.21	0.22
Shear	Avg	0.96	1.07	0.77	1.05	0.99	0.55	0.98	1.09	0.82	1.00	0.85	0.80
	COV	0.26	0.33	0.37	0.25	0.19	0.32	0.16	0.16	0.24	0.15	0.21	0.24
	N° (%)	164 (65%)	127 (50%)	210 (83%)	65 (39%)	67 (40%)	149 (90%)	45 (66%)	28 (41%)	63 (93%)	43 (47%)	27 (29%)	65 (71%)
Bending	Avg	1.09	1.13	1.00	1.03	1,03	0.86	1.05	1.11	1.08	1.02	1.05	0.92
	COV	0.24	0.27	0.13	0.33	0.36	0.10	0.11	0.13	0.11	0.17	0.18	0.14
	N° (%)	88 (35%)	125 (50%)	42 (17%)	101 (61%)	99 (60%)	17 (10%)	23 (34%)	40 (59%)	5 (7%)	49 (53%)	65 (71%)	27 (29%)

experimental evidence, capturing correctly the influence of several parameters, resulting in a reliable method to estimate the capacity of the 4 structural systems analyzed in this paper.

5. Conclusions

In the present work a closed-form model is developed to predict the shear strength of short walls, deep beams, corbels and beam-column joints. This model is based on a reinforced concrete panel element with average strains and stresses, which covers the section of the structural element subjected to shear stress concentration. In addition, the panel element considers longitudinal force equilibrium (the original formulation requires solving this equation by iterations) that allows calibrating strain expressions. Also, a new principal direction angle is calibrated, which covers the elements analogous to cantilever walls (short walls in cantilever, deep beams and corbels). With this, a method is developed to obtain the capacity of the structural element for four limit states that are part of the model (concrete in tension and compression and yielding of longitudinal and boundary reinforcement). Finally, one of the normal strains of the model is calibrated using the least squares method with respect to relevant parameters of the phenomenon, in order to develop expressions, for each limit state, that deliver a closed-form solution for the proposed model.

Thus, for the closed-form general model a predicted to experimental capacity ratio V_{model}/V_{test} yields an average of 1.0 and a COV of 0.25, with similar performances for all four structural systems. When comparing these results with the general model that requires an iterative method, a similar performance is observed. Thus, the developed closed-form model allows maintaining the performance of the initial model, capturing the physics of the analyzed phenomenon.

In comparison to the ACI 318, the proposed model shows better performance, with a better average of the shear strength ratio and a lower COV, for each structural system. For the proposed model, the average strength ratio does not exceed 5% of the perfect correlation (1.0) for each structural system for shear failure, which is lower than what is observed with the AASHTO expression (15%), with similar COV. Considering the simplicity of the model and that its formulation is based on the overall physics of the problem, these results validate the proposed model as a useful tool for estimating the shear capacity of a variety of elements such as short walls, deep beams, corbels and beam-column joints.

References

[1] ACI Committee 318. Building code requirements for reinforced concrete (ACI 318-63). Detroit, Mich: American Concrete Institute; 1963.

[2] Elstner RC, Hognestad E. Laboratory investigation of rigid frame failure. ACI J Proc 1957;53(1):637–68.

[3] ACI Committee 318. Building Code Requirements for Reinforced Concrete (ACI 318-95) and Commentary (ACI 318 R-95). Detroit, Mich: American Concrete Institute; 1995.

[4] Collins MP, Mitchell D, Adebar P, Vecchio FJ. A general shear design method. ACI Struct J 1996;93(1):36–45.

[5] Vecchio FJ, Collins MP. The modified compressional-field theory for reinforced concrete elements subjected to shear. J Am Concr Inst 1986;83(22):219–31.

[6] Vecchio FJ. Nonlinear finite element analysis of reinforced concrete membranes. J Am Concr Inst 1989;86(1):26–35.

[7] Hsu TTC, Mo YL. Softening of concrete in low-rise shearwalls. ACI J Proc 1985;82(6):883–9.

[8] Hwang SJ, Fang WH, Lee HJ, Yu HW. Analytical model for predicting shear strength of squat walls. J Struct Eng 2001;127(1):43–50.

[9] Kassem W, Elsheikh A. Estimation of shear strength of structural shear walls. J Struct Eng 2010;136(10):1215–24.

[10] Massone LM, Ulloa MA. Shear response estimate for squat reinforced concrete walls via a single panel model. Earthq Struct 2014;7(5):647–65.

[11] Massone LM, Álvarez JE. Shear strength model for reinforced concrete corbels based on panel response. Earthq Struct 2016;11(4):723–40.

[12] Massone LM, Orrego GN. Analytical model for shear strength estimation of reinforced concrete beam-column joints. Eng Struct 2018.

[13] Zhang LXB, Hsu TTC. Behavior and analysis of 100 MPa concrete membrane elements. J Struct Eng 1998;124(1):24–34.

[14] Gupta A, Rangan BV. High-Strength Concrete (HSC) structural walls. ACI Struct J

1998;95(2):194–205.
[15] Massone LM. Strength prediction of squat structural walls via calibration of a shear–flexure interaction model. Eng Struct 2010;32(4):922–32.
[16] Wang G, Dai JG, Teng JG. Shear strength model for RC beam–column joints under seismic loading. Eng Struct 2012;40:350–60.
[17] Melo F. Closed-form nonlinear model validation for shear strength estimation of RC short walls, deep beams, corbels and beam-column joints (in Spanish). Civil Engineering Thesis 2017. University of Chile; 2017.
[18] ACI Committee 318. Building Code Requirements for Structural Concrete (ACI 318-14) and Commentary (318R - 14). American Concrete Institute 2014. Farmington Hills, Mich.
[19] Massone LM, Gotschlich NJ, Kang THK, Hong SG. Shear – flexural interaction for prestressed self-consolidating concrete beams. Eng Struct 2013;56:1464–73.
[20] AASHTO LRFD Bridge Design Specifications. American Association of State Highway and Transportation Officials. Washington, D.C.; 2012.